GRAIN FRICTION CONTROLS CHARACTERISTICS OF SEISMIC CYCLE IN ROUGH FAULTS WITH GRANULAR GOUGE

Authors:

I. Omid Dorostkar[1,2]*

1. Chair of Building Physics, Department of Mechanical and Process Engineering, Swiss Federal Institute of Technology Zürich (ETH Zürich), Stefano-Franscini-Platz 1, CH-8093 Zürich, Switzerland
2. Swiss Federal Laboratories for Materials Science and Technology (Empa), Überlandstrasse 129, CH-8600 Dübendorf, Switzerland

*Corresponding author:

Email: domid@ethz.ch Phone: +41587654106

ID: orcid.org/0000-0002-7758-4919

II. Jan Carmeliet[1]

1. Chair of Building Physics, Department of Mechanical and Process Engineering, Swiss Federal Institute of Technology Zürich (ETH Zürich), Stefano-Franscini-Platz 1, CH-8093 Zürich, Switzerland

Email: cajan@ethz.ch

This is a non-peer reviewed preprint submitted to EarthArXiv. The manuscript is submitted to Journal of Geophysical Research (JGR), Solid Earth for possible publication.

Abstract:

Mature faults with rough surface at their core contain granular gouge, however, the presence of fault gouge is mostly disregarded in the analysis of effect of fault's surface roughness on the mechanics and stability of faults. In this work, we consider a rough fault system with constant roughness at the wall-gouge interaction and study the effect of grain friction on the characteristics of seismic cycles. Our discrete element simulations show that the stick-slip frictional strength and dilation of the rough fault system, as well as their variations, nonlinearly increase with the particle friction, but at high particle friction saturate. By statistical analyses on a large number of slip events, we find that the average recurrence time and its variations decrease with particle friction. A rough fault with higher grain friction shows more small slip events, but also contains a limited number of extreme events and demonstrates a more complex nucleation phase with higher stored energy. We analyze the pseudo acoustic emission, which is based on monitoring of the velocity signal of particles, and find higher temporal and more spatially distributed acoustic emissions for rough fault with higher grain friction. Our findings in this study show that, in rough faults with granular gouge, where the fault zone walls are totally engaged to the granular gouge, the friction at grain scale controls the characteristics of stick-slip cycles showing similar influence on the mechanics of faults as the roughness of fault's surface in absence of fault gouge.

Keywords: friction, roughness, stick-slip, granular materials, fault gouge, fault mechanics

1- Introduction

Mature faults at their core are usually characterized by a granular gouge layer, created by wear, communition and other frictional processes in nature [Engelder, 1974; Shimamoto, 1979; Chester et al., 1985; Chester & Logan, 1986; Marone et al., 1990; Chester & Chester, 1998; S. Cashman & Cashman, 2000; Chester & Chester, 2000; Faulkner et al., 2003; Heermance et al., 2003; S. M. Cashman et al., 2007; Zoback et al., 2010]. Characteristics of slip events in laboratory stick-slip experiments including stress drop, pre-seismic friction, recurrence time, compaction etc. have been studied widely for different loading configurations and particle properties [Dieterich & Kilgore, 1994; Chris Marone, 1998; Karner & Marone, 2000; Mair et al., 2002; Brantut et al., 2008; Rathbun & Marone, 2010; Haines et al., 2014; Rosenau et al., 2017]. It is shown that frictional strength and stability of a sheared granular zone are sensitive to grain shape, particle size distribution and their evolution [Mair et al., 2002; Anthony & Marone, 2005].

The stability and slip behavior of natural faults and their relation with fault properties, and in particular their geometry and surface roughness, have been under debate during last years. The fault roughness spans from microns to tens of kilometers [Kozłowska et al., 2018] and can be measured using different methods [Renard et al., 2006; Sagy et al., 2007; Candela et al., 2009; Bistacchi et al., 2011; Emily E. Brodsky et al., 2011; Candela et al., 2012; Emily E Brodsky et al., 2016]. At field scale, the fault roughness is suggested to control the stress drop and slip distribution during earthquakes, hydraulic fracturing and subduction of seafloor relief [Bouchon et al., 2010; Candela, Renard, Bouchon, et al., 2011; Candela, Renard, Schmittbuhl, et al., 2011; Wang & Bilek, 2014; Rijsingen et al., 2018]. At lab scale, experimental studies showed that the topology and fault structure influence the spatial and temporal distribution of small and large earthquakes [Ohnaka & Shen, 1999; Ohnaka, 2003; T. H. W. Goebel, Becker, et al., 2014; Thomas H.W. Goebel et al., 2017]. Numerical simulations have been also used to study the effect of fault roughness on mechanics and nucleation of slip events [Chester & Chester, 2000; Dieterich & Smith, 2009; Angheluta et al., 2011; Dunham et al., 2011; Fournier & Morgan, 2012; Rathbun et al., 2013; Bruhat et al., 2016; Zielke et al., 2017; Tal & Hager, 2018; Tal et al., 2018].

However, the presence of granular fault gouge is neglected in most of the previous studies related to fault roughness. The study of Rathbun et al. [2013], considered the presence of fault gouge during stable sliding simulations and found that, on the first-order, fault strength is controlled by particle friction and mechanical coupling of the fault zone wall to the gouge for both rough and smooth faults. Rathbun et al. [2013] showed that, for rough faults, when the fault zone walls and gouge zone are totally engaged with no slip between them, only the gouge friction controls the strength. In this work, we systematically vary the particle friction coefficient (called here for simplicity particle friction) in a fault with granular gouge and focus on stick-slip dynamics to study the effect of particle friction on the slip size distribution and inter-event time of seismic cycles describing the micromechanical properties of frictional processes that take place in the fault damage zone. To this end, we perform 3-D DEM simulations recording hundreds of slip events for statistical analyses provided by the advantage of numerical simulations. We also study the evolution of elastic strain energy (i.e. potential energy in [Dorostkar, 2018; Dorostkar & Carmeliet, 2018]), kinetic energy, and the micromechanics of slip events and explain the macro-scale response of fault with grain-scale metrics (e.g. [Dorostkar, Guyer, et al., 2017a]). Using a simple rheological and geometrical granular contact model, we will show that, although our simplified numerical approach does not contain all complexities present in nature, it shows that for faults with granular gouge, the friction of the gouge particles controls the characteristics of stick-slip cycles. We also compare our findings with previous numerical and experimental works and show that, in rough faults with granular gouge, the friction at grain scale has similar influence on the mechanics of faults as the roughness at fault's surface in absence of fault gouge.

2- Model description

Due to particulate nature of granular fault gouge, we use DEM to model gouge grains. In DEM, the equations of motion solved for each particle considering the applied forces are:

$$\sum F_p = m(\frac{d}{dt}u_p), \quad (1)$$

$$\sum T_p = I(\frac{d}{dt}\omega_p), \quad (2)$$

where m, I, u_p and ω_p are the mass, the moment of inertia and the translational and angular velocity of particle, respectively. In Eq. (1) and (2), F_p and T_p are the forces and torques acting on particle *i* owing to particle-particle contacts. In soft sphere DEM, the particle-particle contact allows an overlap between them and the contact law is described by a combination of different rheological elements (spring, dashpot, slider etc.). These elements are at play when particles are in contact. Upon contact loss, there are no contact forces acting between the particles. In order to capture particle scale nonlinearity, we use the nonlinear Hertzian contact law. In this particle-particle contact law, the spring stiffness and the coefficient of damping are function of particle material properties and the overlap between particles [Hertz, 1882; Di Renzo & Di Maio, 2004]. The normal and tangential contact forces are calculated as follows:

$$F_{pn} = -k_{pn}\delta\varepsilon_{pn} + c_{pn}\delta u_{pn} \,, \tag{3}$$

$$F_{pt} = \min\left\{\left|k_{pt}\int_{t_{c,0}}^{t} \delta u_{pt}\, dt + c_{pt}\delta u_{pt}\right|, \mu_c F_{pn}\right\}, \tag{4}$$

where k_{pn} and k_{pt} are the normal and tangential spring stiffness, c_{pn} and c_{pt} are the normal and tangential damping coefficient, $\delta\varepsilon_{pn}$ is the overlap and δu_{pn} and δu_{pt} are the relative normal and tangential velocities of two particles in contact, respectively. In Eq. (4), the parameter μ_c represents the particle friction coefficient that limits the tangential force. When the tangential contact force between two particles in contact reaches this limit, they start sliding against each other. The integral term in Eq. (4) shows an incremental spring, storing energy based on the relative elastic tangential deformation of the particle surface starting from the moment particles touch each other at $t_{c,0}$. A damping is added to the spring component of the tangential force if the Coulomb criterion is not met [Di Renzo & Di Maio, 2004; Goniva et al., 2012]. The spring and damping coefficients are calculated as follows:

$$k_{pn} = \frac{4}{3} Y^* \sqrt{R^* \delta\varepsilon_{pn}} \, , \tag{5}$$

$$k_{pt} = 8 \, G^* \sqrt{R^* \delta\varepsilon_{pn}} \, , \tag{6}$$

$$c_{pn} = -2 \sqrt{\frac{5}{6}} \times \frac{\ln(r)}{\sqrt{ln^2(r)+\pi^2}} \times \sqrt{2Y^* \sqrt{R^* \delta\varepsilon_{pn}} \, m^*} \, , \tag{7}$$

$$c_{pt} = -2 \sqrt{\frac{5}{6}} \times \frac{\ln(r)}{\sqrt{ln^2(r)+\pi^2}} \times \sqrt{8 \, G^* \sqrt{R^* \delta\varepsilon_{pn}} m^*} \, , \tag{8}$$

where, r is the restitution coefficient, and Y^*, R^*, G^* and m^* are the equivalent Young's modulus, radius, shear modulus and mass, respectively, calculated as follows:

$$\frac{1}{Y^*} = \frac{(1-\upsilon_1^2)}{Y_1} + \frac{(1-\upsilon_2^2)}{Y_2} \, , \tag{9}$$

$$\frac{1}{G^*} = \frac{2(2-\nu_1)(1+\nu_1)}{Y_1} + \frac{2(2-\nu_2)(1+\nu_2)}{Y_2} \, , \tag{10}$$

$$\frac{1}{R^*} = \frac{1}{R_1} + \frac{1}{R_2} \, , \tag{11}$$

$$\frac{1}{m^*} = \frac{1}{m_1} + \frac{1}{m_2} \, , \tag{12}$$

where subscripts 1 and 2 refer to the two particles in contact and υ is the Poisson's ratio of the particle.

Figure 1 illustrates a granular layer representing a part of a granular fault gouge. In our model, 8000 spherical particles constitute this layer with particle diameter ranging 90-150 μm having a uniform, poly-disperse particle size distribution. The sample size in our simulations is 11×1.5×0.8 mm^3. In order to model a fault with rough surface in a simplified way, on the sample top and bottom, we employ two corrugated plates with high surface roughness modeled by a friction coefficient of 0.9 between the plates and particles to facilitate the transmission of shear stresses to the granular gouge (see Fig.1 insets). This kind of geometry is inspired from the BIAX laboratory earthquake machine using corrugated driving blocks [Chris Marone, 1998; Rivière et al., 2018] and simulates a fault system with rough surface. Our analysis shows that use of these corrugated plates with high surface friction leads to a total engagement of fault blocks with granular gouge. Therefore, no slip takes place at the boundary between the plates and the granular gouge, but the deformation is distributed across the sample thickness, inside the granular gouge (see Fig. 13). In this paper, our study is dedicated to the influence of the gouge particle friction on stick-slip behavior and we do not study the effect of fault roughness i.e. characteristics of the corrugated plates e.g. length, depth, etc. on the dynamics of the sheared granular layer. A detailed analysis showed that change of these characteristics does not fundamentally alter the dynamic regime of stick-slip. Rathbun et al. [2013] showed that, due to a better engagement between the corrugated plates and gouge zone, a higher roughness of corrugated plates characterized with larger tooth size will extend the deformation more inside the gouge zone [Rathbun et al., 2013]. The previous research showed that by increasing the rolling friction i.e. the resistance of particles to rotate, the stick-slip dynamics becomes more stabilized and the dynamic regime tends to change from stick-slip to slow slip, defined as a more gradual decrease of the macroscopic friction rather than a sudden drop [Dorostkar, 2018].

Therefore, since our focus here is on stick-slip dynamics and we aim to isolate the effect of particle friction in a detailed analysis, we do not include the effect of rolling resistance and consider it zero within the scope of this manuscript.

On the front- and back-side of the sample, we implement frictionless walls with the same elastic properties of particles. This type of interaction between particles and walls are designed to avoid rigid wall boundary conditions. Wall-particle interaction in our DEM model is the same as particle-particle interaction when one particle has an infinite radius. Periodic boundary conditions are applied at the left and right sidewalls representing a long fault gouge in x direction. The periodic boundary conditions allow for large shear displacements, and facilitate recording many slip events to be used for statistical analyses. To prepare the sample, particles are inserted randomly in space descending with an initial velocity of 10^{-2} cm/s. Next, the upper plate is moved downward to apply a confining stress to confine the sample (applied on top x-y plane in Fig.1). At this stage, the load increases until the desired confining stress is attained (10 MPa). The position of the upper plate is adapted continuously, as in the lab experiments, in order to maintain the confining stress constant. At constant confining stress, shearing is initiated by moving the bottom plate in x direction with a displacement-controlled mechanism (constant velocity of 600 μm/s) until reaching the maximum shear stress, at which point the stick-slip process commences. The particle density is 2900 kg/m^3 that results in an applied time step of 15×10^{-9} seconds for DEM calculations, within the recommended range based on the Rayleigh time. Our DEM calculations remain in the quasi-static regime by controlling the inertial number to be below 10^{-3} [MiDi, 2004; Sheng et al., 2004; Agnolin & Roux, 2007]. Similar to our previous works [Dorostkar, Johnson, et al., 2017; Dorostkar et al., 2018], we use LIGGGHTS [Goniva et al., 2012; Kloss et al., 2012] to model the granular fault gouge.

3- Results

We show in Fig. 2a and 2b the evolution of macroscopic friction and gouge thickness during the stick-slip dynamics, respectively, for three different particle friction values of 0.1, 0.5 and 0.9. The macroscopic friction is defined as the ratio of shear stress to normal stress (confining stress) on the driving block and the gouge thickness represents the measurement in z direction of Fig. 1. All simulations start from the same initial thickness and particle arrangement. Figure 2c shows with higher resolution the shaded area in Fig. 2a. The macroscopic friction rapidly increases in the sample and after some stable sliding; the sample undergoes stick-slip dynamics, where the start of stick-slip dynamics is denoted by time zero. For each stick-slip cycle, the macroscopic friction (or shear stress, since the confining stress is kept constant) increases nonlinearly reaching to a critical state where micro-slips take place followed by a major slip event. The average macroscopic friction increases nonlinearly with the particle friction: at low particle friction values (0.1 to 0.5), the macroscopic friction increases much more compared to high particle friction values (0.5 and 0.9). A similar behavior can be observed for the gouge thickness (Fig. 2b).

The schematic stick-slip cycle shown in Fig. 3a shows the definition of recurrence time, micro-slips and major slip event in our analysis. We recognize major slip events with a drop in macroscopic friction larger than or equal to 0.01, a threshold that avoids capturing micro-slips before a major slip event [Dorostkar, Guyer, et al., 2017b]. We perform long simulations and measure the average macroscopic friction, gouge thickness and slip recurrence time over all stick-slip phases as function of particle friction (Fig. 3b-d). We observe that the gouge strength represented by macroscopic friction increases nonlinearly with particle friction and saturates at around $\mu_c = 0.9$ to 1. A similar behavior is observed for gouge thickness (Fig. 3c). The standard deviations of macroscopic friction signal and gouge thickness are found to increase with increasing particle friction (Fig. 3b and 3c). The slip recurrence time and its standard deviation decreases with increasing particle friction, meaning that slip events occur more often and more regularly in a gouge with higher frictional particles (Fig. 3d)

To complement the observations in Fig. 3, in Fig. 4a, we observe an almost linear relation between macroscopic friction and gouge thickness for simulations with different particle friction. The more dense population of data points at higher thickness and macroscopic friction is consistent with the nonlinear behavior observed in Figs. 2b and 2c. We also observe that the number of slip events increases with increasing particle friction (equivalent to a decreasing recurrence time as seen in figure 3d). The histogram of slip events' friction drop (Fig. 5) shows that this increase in number of events at higher particle frictions mainly stems from smaller events. This implies that, a fault gouge with higher particle friction experiences more smaller slip events at a shorter and more regular inter-event time (less standard deviation in

Fig. 3d) with lower friction drop. Remark however that, at high particle friction, although the majority of the slip events are smaller, there are also some extreme slip events, which are larger than the events at lower particle friction.

When studying the time evolution of the average contact force, we find a similar stick-slip type of behavior (Fig. 6). This observation shows that the contact forces at grain scale control the macroscopic response of the sheared granular gouge. We observe that, by increasing the particle friction, the average contact force increases, however the relative increase of higher particle friction becomes smaller at higher values. The decomposition of contact force into normal and tangential components shows that the contribution of the normal component is dominant irrespective of particle friction value. The relative contribution of normal contact force to the total contact force compared to the contribution of the tangential contact force, however, decreases for higher particle frictions.

The Slipping Contact Ratio (SCR) is defined as the ratio between number of contacts at Coulomb frictional limit prone to slip and the total number of contacts. In Fig. 7a, we observe drops in SCR of almost one order of magnitude when changing the particle friction from 0.1 to 0.5 or from 0.5 to 0.9. At the same time, Fig. 7b shows that the average coordination number (coordination number is the number of contacts per particle) decreases with increasing particle friction. The decrease in coordination number for higher particle frictions can be attributed to the larger dilation or higher gouge thickness (see Fig. 2b). We remark that, since the coordination number decreases with increasing particle friction (Fig. 7b), we also check the total number of slipping contacts that is not normalized by the number of contacts and observe similar behavior: the total number of slipping contacts decreases with increasing particle friction.

In Figs. 7c and 7d, we show the instantaneous and cumulative particle displacement averaged over all particles, respectively. The cumulative displacement is the total displacement of a particle from the start of each simulation. The instantaneous particle displacement shows larger jumps upon micro- or major slips for higher particle frictions. Moreover, the cumulative particle displacement clearly shows that for a given instant in time (or a given shear strain), particles with higher particle friction have undergone higher total displacements. Our analysis shows that particle displacement is mainly in x-direction (99 %) along the moving boundary that imposes the shear stress (Fig. 1).

We also study the evolution of potential and kinetic energies in sheared granular fault gouge (Fig. 8). The elastic strain potential energy is stored within the particle-particle contacts through overlap between particles [Dorostkar & Carmeliet, 2018] and the kinetic energy is due to translation and rotation of particles. The fault gouge with higher particle friction shows more potential energy, however, the increase in average potential energy is not linear with respect to the increase of particle friction. For instance, an increase of particle friction by a factor 9, from 0.1 (Fig. 8c) to 0.9 (Fig. 8a), leads to an increase in potential energy only by a factor 3. We also observe that the kinetic energy signal for higher particle frictions shows more fluctuations and bursts i.e. important rearrangements of particles inside the fault gouge. While the potential energy at low particle friction (Fig. 8c) shows a plateau before the major slip events, the energy is always increasing approaching slip events for higher particle frictions (Fig. 8a).

We compare in Fig. 9 the evolution of macroscopic friction and gouge thickness for particle frictions with 2 orders of magnitude contrast i.e. 10, 1 and 0.1. The nucleation phase of slip events for higher particle friction (Fig.9a) shows a complex behavior in both macroscopic friction and gouge thickness signals, where a considerable amount of small drops in macroscopic friction occur during the stick phase before an upcoming extreme slip event that has a long recurrence time. The statistical analysis of the size of all slip events based on drop in macroscopic friction (Fig. 10) shows that slip events occur more often for higher particle frictions i.e. larger number of slip events with shorter recurrence interval. More importantly, we observe that, although the higher number of slip events stems mainly from smaller events (see also Fig. 5), there exist also some very large slip (extreme) events (Fig. 10).

Our analyses show that the velocity (or acceleration) signal of a flagged particle, which is called "pseudo Acoustic Emission (AE)" signal in this study, demonstrates (Fig. 11a) a very similar behavior to acoustic data of the lab (e.g. [Rouet-Leduc et al., 2017]). We will discuss the details of this observation in Section 4. In Fig. 11b, the velocity signal of a flagged particle shows bursts at slip events, which are larger for higher particle frictions. The complementary Cumulative Distribution Function (cCDF) of pseudo acoustic emission bursts (for all emissions without threshold, during both stick and slip phases) in Fig. 12 clearly shows the increase of AE amplitude for higher particle frictions. We remark that the observations in Fig. 11 and 12 are not dependent on the flagged particle and are recorded consistently for several chosen particles.

We further look at the micromechanics of fault by visualizing the particles on a plane representative of the whole box (here the front x-z plane of the gouge in Fig. 1) for particle friction values of 0.1 and 10, at a point during the stick phase (Fig. 13). For panels a and b, we set the maximum of color bar equal to the shear driving plate velocity, 0.06 cm/s. While a gradient is observed for particle friction of 0.1 from top to bottom, where the particles close to the bottom plate have velocity close to 0.06 cm/s, the particle velocity field shows a more uniformly distributed profile for a particle friction of 10. We will discuss the implications of this observation in Section 4. A comparison between panels c and d shows a larger cumulative displacement for particles with particle friction of 10, where the maximum of color bar is set to the maximum cumulative displacement of particles with particle friction of 0.1, for a better comparison. It is clear from Fig. 13d that a larger portion of the sample has experienced a large displacement. We remind that the main displacement for particles is in x direction, along the driving plate motion. The spatial distributions in panels c and d are consistent with temporal evolution in Fig. 7d. The spatial distributions of coordination number for both particle frictions are rather uniform, while the gouge with lower particle friction shows higher coordination numbers consistent with observations of Fig. 7b. The gouge with higher particle friction shows on average lower numbers, also showing some 'blue' spots with very low coordination number.

4- Discussion

We found that the frictional strength of the sheared granular fault gouge during stick-slip dynamics increases with particle friction, but saturates at particle friction values around 0.9-1 (Fig. 3). The nonlinear macroscopic behavior and saturation of friction are attributed to the rotational behavior of the particles showing a gradual transition from sliding to rolling, since high particle friction makes the conditions easier for particles to roll [J. Latham et al., 2005; Azéma et al., 2012; Shojaaee et al., 2012; Göncü & Luding, 2013; Rathbun et al., 2013; Azéma et al., 2017]. Furthermore, we show a linear relation between macroscopic stick-slip friction and gouge thickness (Fig. 4), as is confirmed by previous research [Mead, 1925; C. Marone, 1998; Frye & Marone, 2002; Knuth & Marone, 2007; Makedonska et al., 2011]. From the micromechanical point of view, we only observed a small increase in tangential contact force, while our results show that, the overall shear strength of fault gouge increases at higher particle friction. This means that the increase in shear strength cannot be attributed to the increase of tangential contact force. In other words, the increase in particle friction leads to an increase in normal contact forces enhancing the shear capacity of the system. To explain this observation, we pose the hypothesis that a structural effect is introduced, where at higher particle friction less slipping contacts occur, providing a better support for a contact network to build up higher contact forces. The lower number of slipping contacts (or the higher number of locked contacts) could also explain the larger cumulative particle displacement (Fig. 7 and Fig. 13), as rough faults are suggested to require more overall work to shear leading to more deformation in the fault zone [Rathbun et al., 2013]. The hypothesis here is that, the fault gouge with higher particle friction has to undergo more complex states during deformation towards failure, which involves more locked contacts in spite of a lower total number of contacts. This makes the system to experience a wider range of macroscopic frictions and dilations manifested in higher variations of macroscopic friction and gouge thickness (Fig. 3). The system with higher particle friction going through those complex topographical states has to expand more to accommodate the continuous externally applied shear, which leads to a higher dilatation and a lower coordination number. These conditions make a fault gouge with higher particle friction to fail more frequently leading to more fluctuations in both macroscopic friction (slip events) and gouge thickness. A slip event in a sheared granular layer is found to be a phenomenon where the slipping contact ratio increases approaching the failure leading to a major slip event. Therefore, from another point of view, in a system with a higher particle friction and lower slipping contact ratio, the slip event is prevented due to stronger contacts, so that the system will only partially fail leading to a large number of smaller slips. We also remark that, since the main displacement for particles is along the direction of the shear driving plate (x direction in Fig. 1), the higher cumulative particle displacement for a higher particle friction is consistent with a higher number of slip events, where at each slip event there is a displacement (rupture) for the center of mass of the granular fault gouge.

Based on our observations, we argue that the effect of gouge particle friction on the mechanics of faults and characteristics of seismic cycles has a similar effect as increasing the fault roughness in absence of fault gouge. The recent numerical model using 2-D plane strain calculations by Tal and Hager [2018] showed that, as the fault surface roughness amplitude increases, the load in the fault is released by more slip events but with lower average stress drops [Tal & Hager, 2018]. Similarly, we observe in Fig. 4 that increase of particle friction leads to more slip events but with lower friction drops. Furthermore, using numerical simulations, Tal et al. [2018] observed a more complex behavior for faults with higher roughness, where the complexities in the nucleation process are reflected as irregular fluctuations in the moment rate for rougher faults [Tal et al., 2018]. We observe a similar complexity in 3D DEM, where the nucleation (stick) phase of slip events contains many fluctuations i.e. smaller slip events. However, using the advantage of DEM and employing the periodic boundary conditions we can shear the fault gouge during long time collecting information of hundreds of slip events. Using a statistical analysis, we then show that a fault gouge with high enough particle friction and large enough shear displacement shows, besides the large amount of small events, some extreme slip events with long recurrence time compared to faults with lower particle friction.

Acoustic emission is suggested to originate from groaning, creaking, and chattering of continuous grain motions and breakage of force chains within the fault gouge during laboratory stick-slip experiments [McLaskey & Glaser, 2011; T. H. W. Goebel et al., 2012; T. H. W. Goebel, Candela, et al., 2014; Thomas H.W. Goebel et al., 2017; Rouet-Leduc et al., 2017; Rivière et al., 2018]. We use the velocity signal of flagged particles as pseudo-acoustic emission signals, however, since the velocity profile of a flagged particle contains both motion from arriving waves owing to rearrangements of other particles and the motion of the particle itself, we call it "pseudo AE" signal. In other words, although our AE signal is derived from the motion of a single flagged particle compared to the lab signal where the AE is usually recorded with a device outside of the fault gouge; we find that the pseudo AE signal contains sufficient information for the purpose of this study, where we compare the velocity signal from the same particles for simulations with different particle frictions. As the experimental work by Kwiatek et al. [2014] showed that the observed changes in AE characteristics are clearly correlated to the fault topography and roughness [Kwiatek et al., 2014], Goebel et al. [2017] discussed that faults with rougher surface show a more spatially distributed AE activity and a higher b-value i.e. the measure for the relative abundance of the strong to the weak earthquakes based on the Gutenberg–Richter law [Thomas H.W. Goebel et al., 2017]. Our DEM simulations show dependency of AE on fault particle friction. We observe higher temporal (Fig. 11 and 12) and more spatially distributed AE (Fig. 13) for fault with higher particle friction. The higher AE in fault gouge with higher particle friction is consistent with more frequent kinetic energy releases (Fig. 8), since AE is believed to originate from the rearrangement of particles. We remind that, although our discussion on AE is based on velocity tracking of single flagged particles, the temporal evolution and higher moments of those signals show very similar behavior to laboratory AE (e.g.

[Rouet-Leduc et al., 2017; Rivière et al., 2018]), as we are using them for machine learning analyses in our ongoing research.

Overall, our observations on the effect of particle friction using 3-D DEM model of a granular fault gouge show similarities to other numerical and experimental works on the effect of fault surface roughness, where the presence of granular gouge has been disregarded. In order to better document this observation, in Fig. 14 we show schematically a fictitious shear plane for gouges with low and high particle frictions. For a rough fault with a granular gouge at the core, where the fault surface is totally engaged with the gouge and deformation (slip) takes place inside the gouge zone, our macro- and micro-scale observations suggest high particle friction originates a more complex topography and shear pattern for slip, which is similar to a surface with high roughness amplitude. This rougher shear pattern stems from stronger granular structure at higher particle friction, showing more locked contacts and the larger deformation that the fault gouge has to go through approaching failure. The DEM model in this work is a vast simplification of real faults in nature but yet expands our understanding of micro-scale fault frictional processes and provides a means to study and measure quantities that are not feasible to measure in the lab and in the field, showing how numerical models can boost our understanding from physical processes that dictate frictional strength of a fault damage zone.

5- Conclusions

We model stick-slip dynamics of a granular fault gouge by 3-D discrete element simulations and study the influence of particle friction on the characteristics of seismic cycles. The major findings of this study can be summarized as follows:

- The fault gouge frictional strength, dilation and their variations nonlinearly increase with particle friction, saturating at high particle friction.
- The average slip events' recurrence time and its variations decrease with particle friction. A fault gouge with higher particle friction shows a more complex nucleation (stick) phase, characterized by many smaller slip events as manifested by the more frequent energy release in the kinetic energy signal.
- Our statistical analyses on a large number of slip events obtained by shearing the fault gouge to a large shear strain suggest that a fault gouge with higher particle friction shows a higher number of slip events mainly consisting in small slip events. However, there are also some extreme slip events larger than the extreme events of fault gouge with lower particle friction.
- The fault gouge with higher particle friction shows higher stored potential energy and stronger particle-particle contacts leading to a structure that needs more work to deform. Therefore, for a given shear strain, the particles in a gouge with higher particle friction experience more deformation.

- The pseudo acoustic emission analysis, based on monitoring the velocity of particles, shows higher temporal emissions for fault gouge with higher particle friction.
- Our observations suggest that, in a rough fault with granular gouge where the rough fault surface is engaged with the gouge zone, the effect of gouge particle friction on the characteristics of seismic cycles is similar to the effect of fault surface roughness in absence of fault gouge.

6- Acknowledgement

The authors thank ETH Zurich for funding this study. The data related to this paper can be obtained by contacting the corresponding author at domid@ethz.ch.

7- Figures

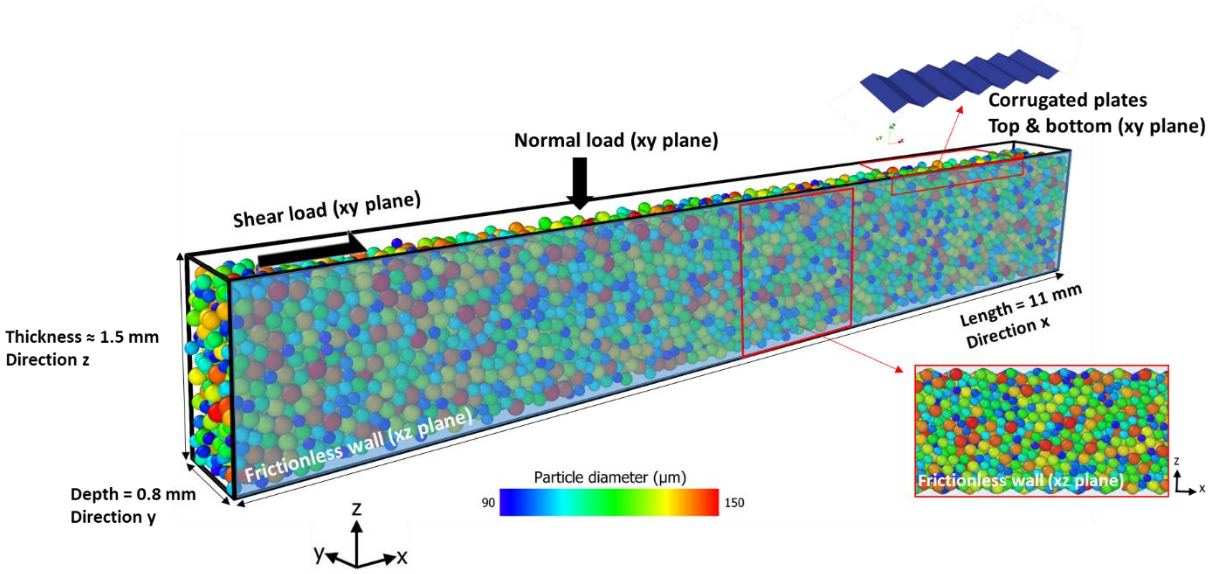

Fig. 1: Three dimensional granular fault gouge with 8000 particles with poly-disperse diameter distribution of 90-150 micrometer. The fault gouge is confined in z direction and sheared in x direction, with periodic boundary conditions at the end on y-z planes. The shear load is applied along the x-y plane. Two corrugated plates are used on top and bottom x-y planes of the gouge to simulate a rough fault surface. The x-z planes are frictionless walls. (Image produced with the open source visualization tool (OVITO) [Stukowski, 2010]).

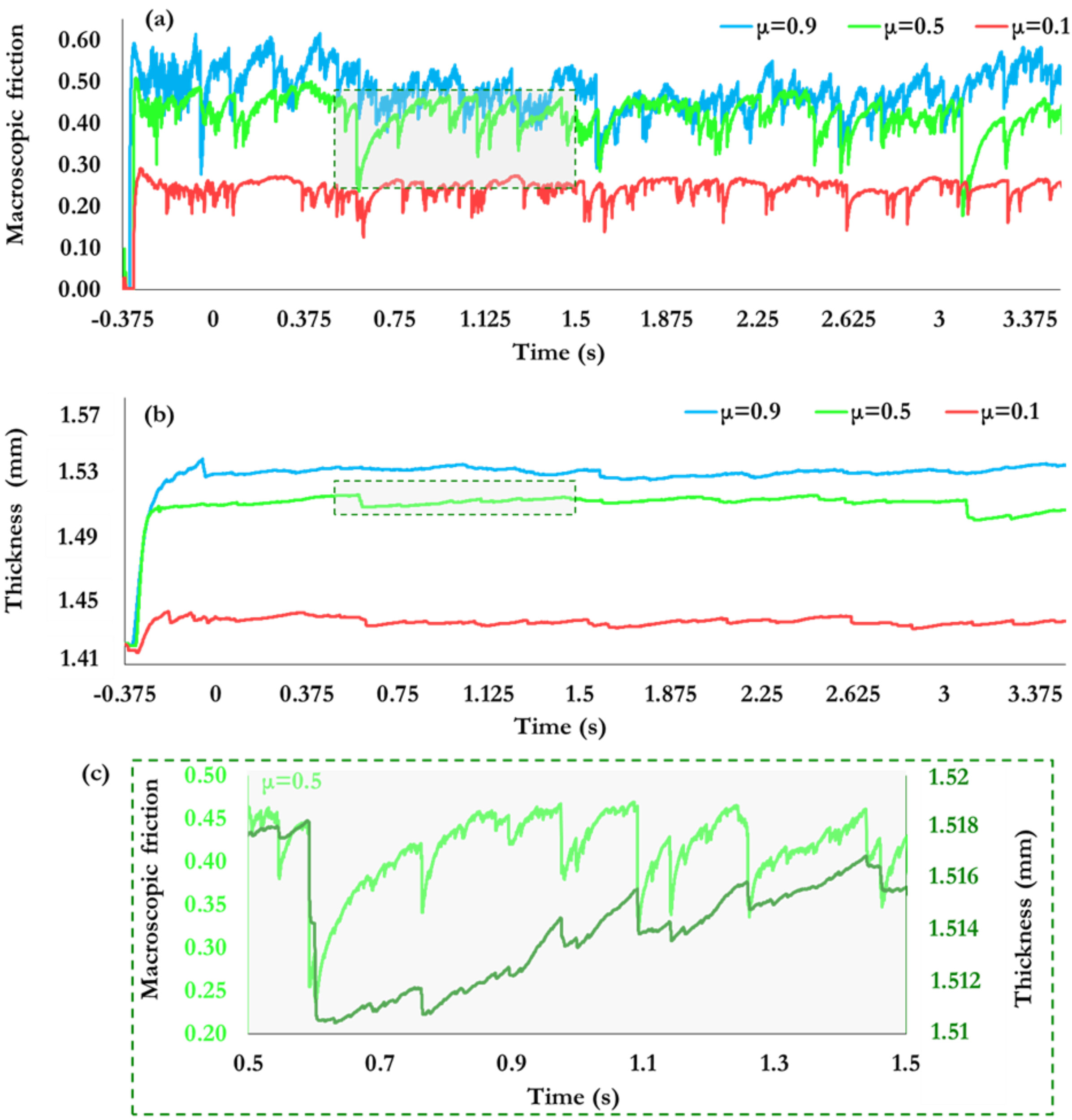

Fig. 2: Time series of (a) macroscopic friction and (b) fault gouge thickness for three different particle friction values. The greenish shaded areas in a and b are shown in (c) with a higher resolution for $\mu = 0.5$. Please note that the thickness is shown with a secondary axis in c. Time zero denotes the start of stick-slip dynamics after the initial stable sliding.

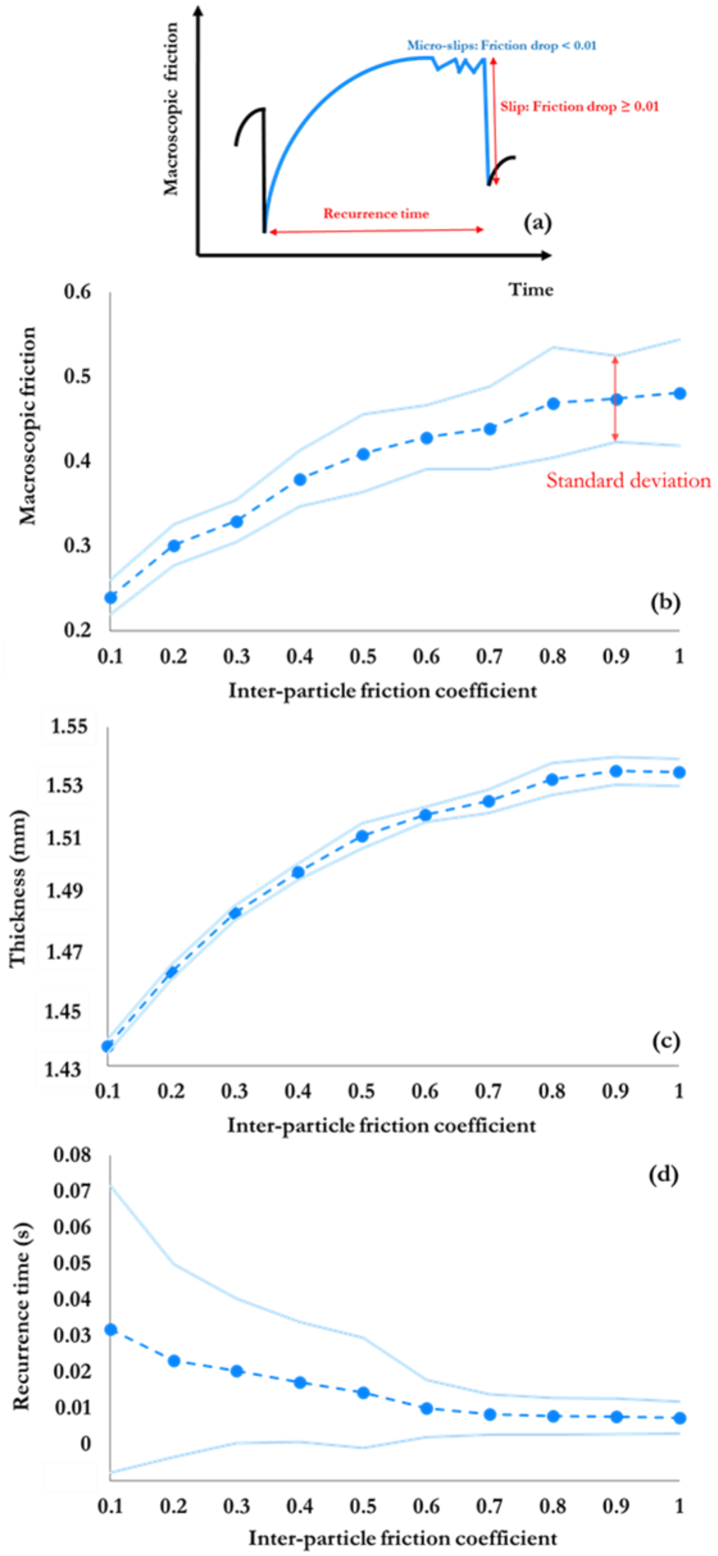

Fig. 3: (a) Schematic showing the definition of slip event, micro-slips and recurrence interval. Average (b) macroscopic friction, (c) fault gouge thickness and (d) slip recurrence time as a function of the particle friction. The light blue lines in b-d show the uncertainty limits based on the standard deviation of data.

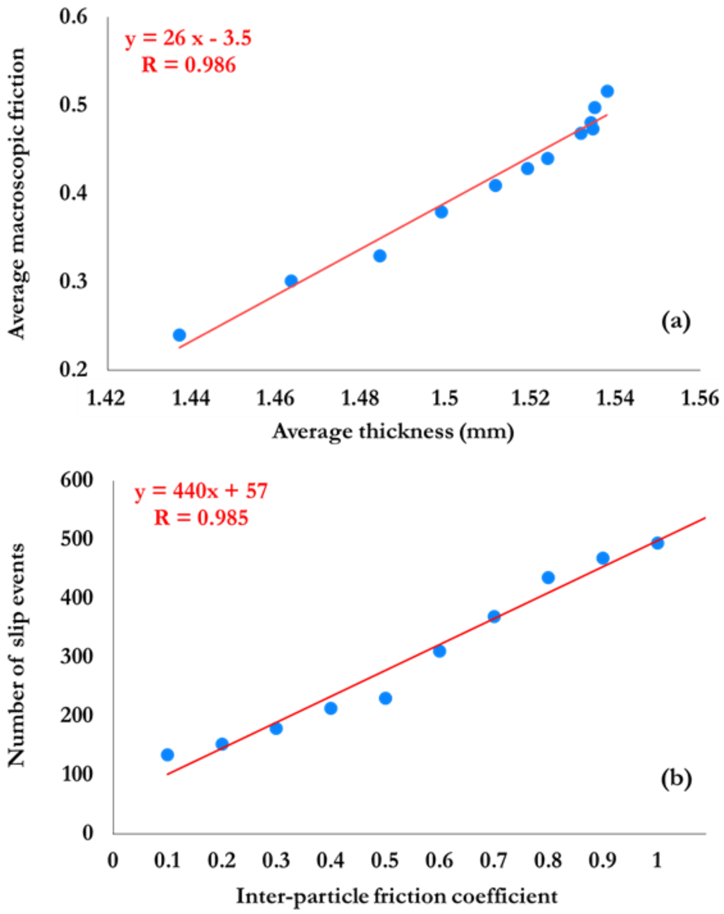

Fig. 4: (a) Average macroscopic friction versus average thickness for stick-slip dynamics with different particle friction values. (b) Number of slip events versus particle friction.

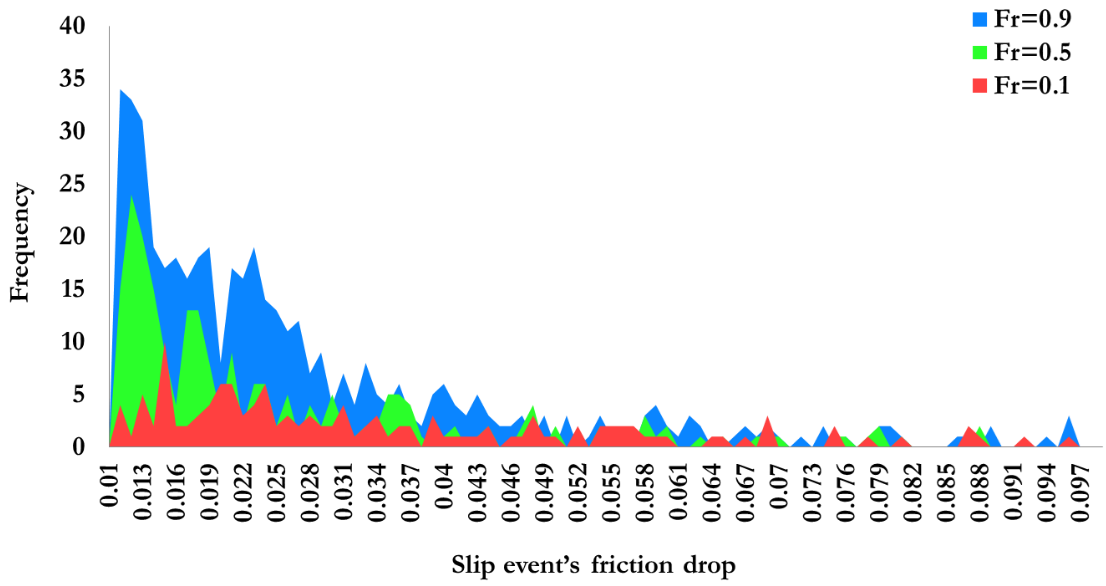

Fig. 5: Histogram of slip event's friction drop for three different particle friction values. The maximum slip event's friction drop in this histogram is limited to 0.1 to highlight and better show the frequency of slip events with small friction drop.

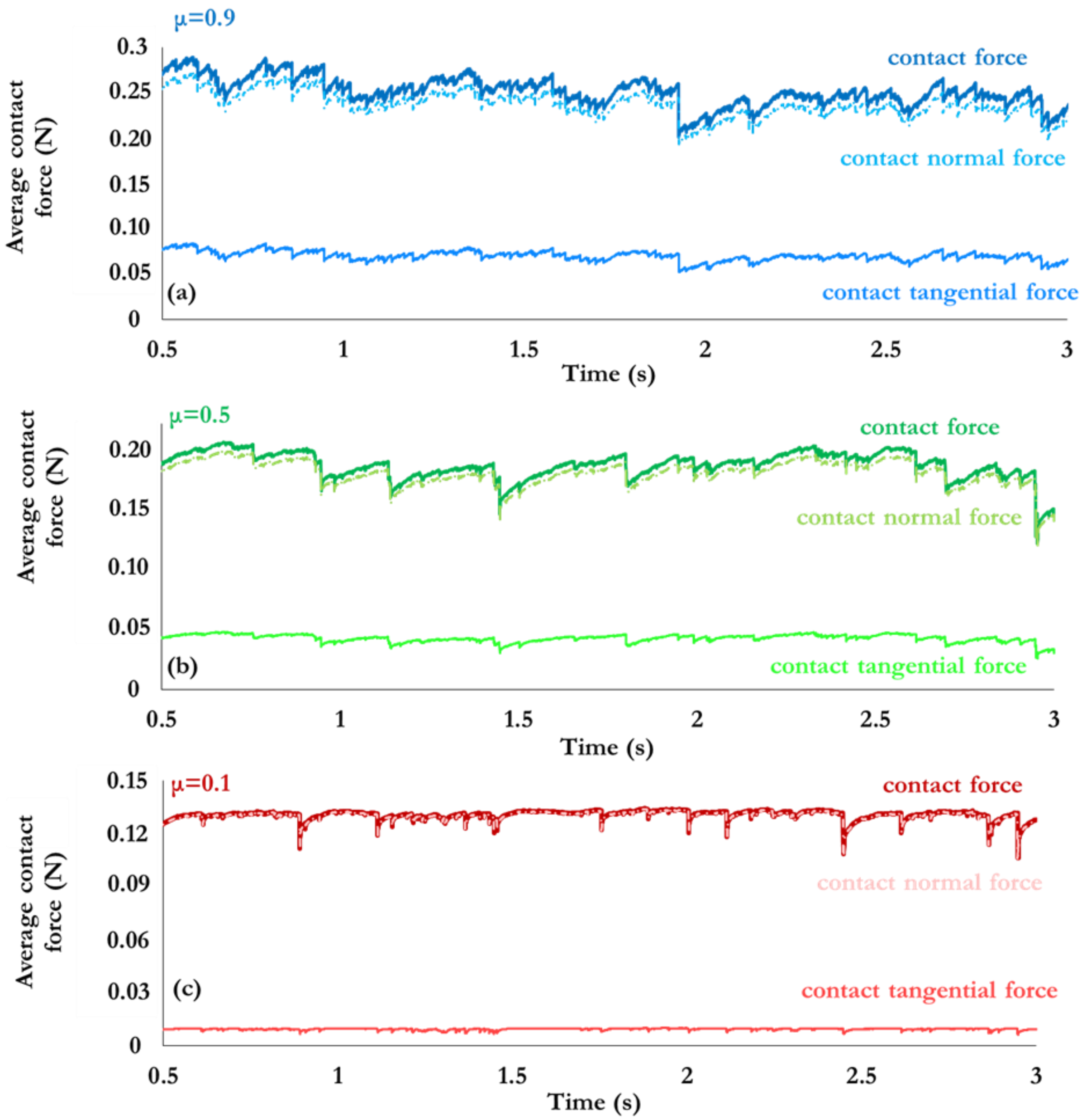

Fig. 6: (a-c) Average contact force for particle friction values of 0.1, 0.5 and 0.9, respectively. In each panel, the components of contact force (normal contact force and tangential contact force) are separately shown.

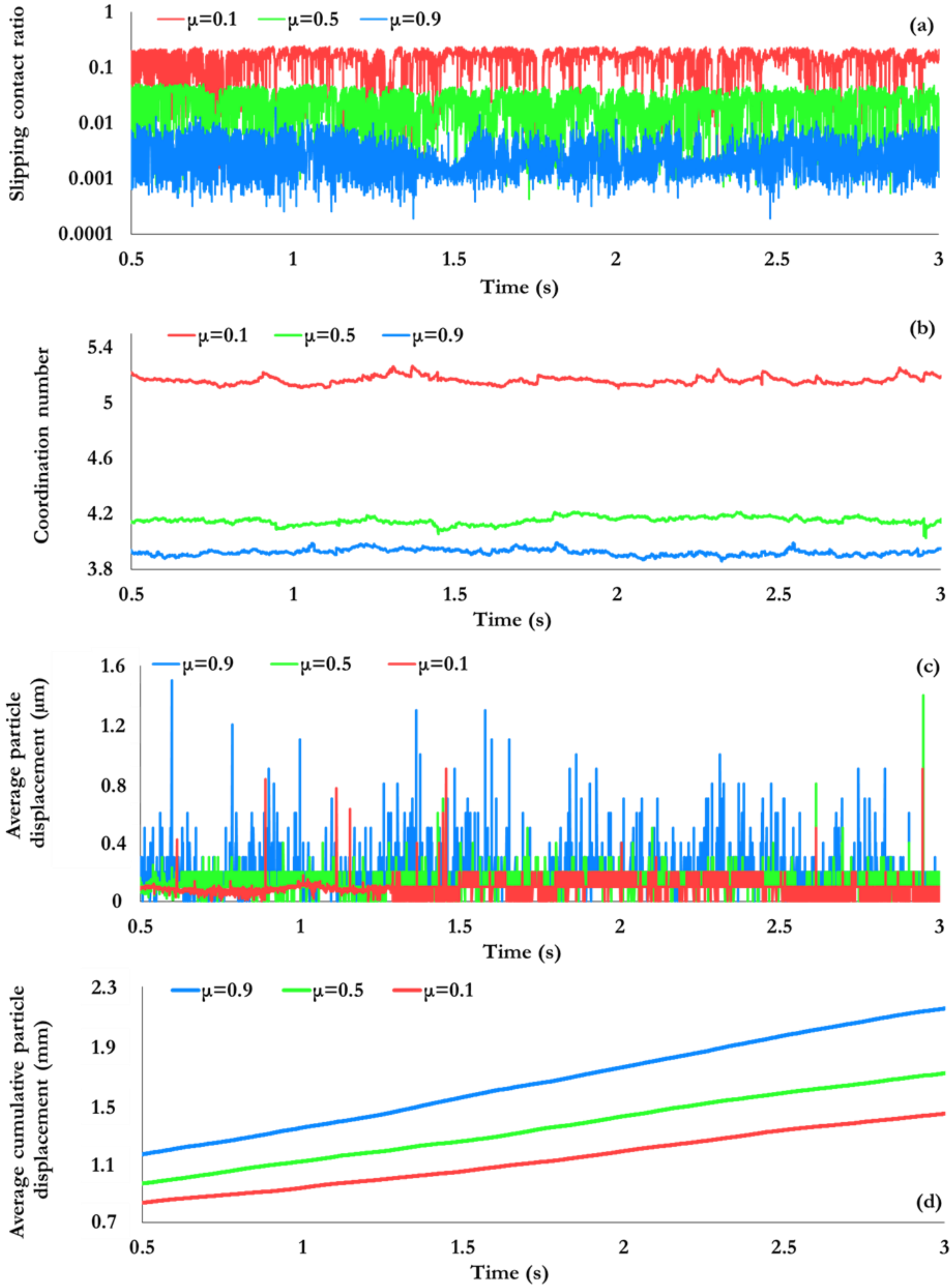

Fig. 7: Time series of (a) slipping contact ratio, (b) coordination number, (c) average particle displacement and (d) average cumulative particle displacement for particle friction values of 0.1, 0.5 and 0.9.

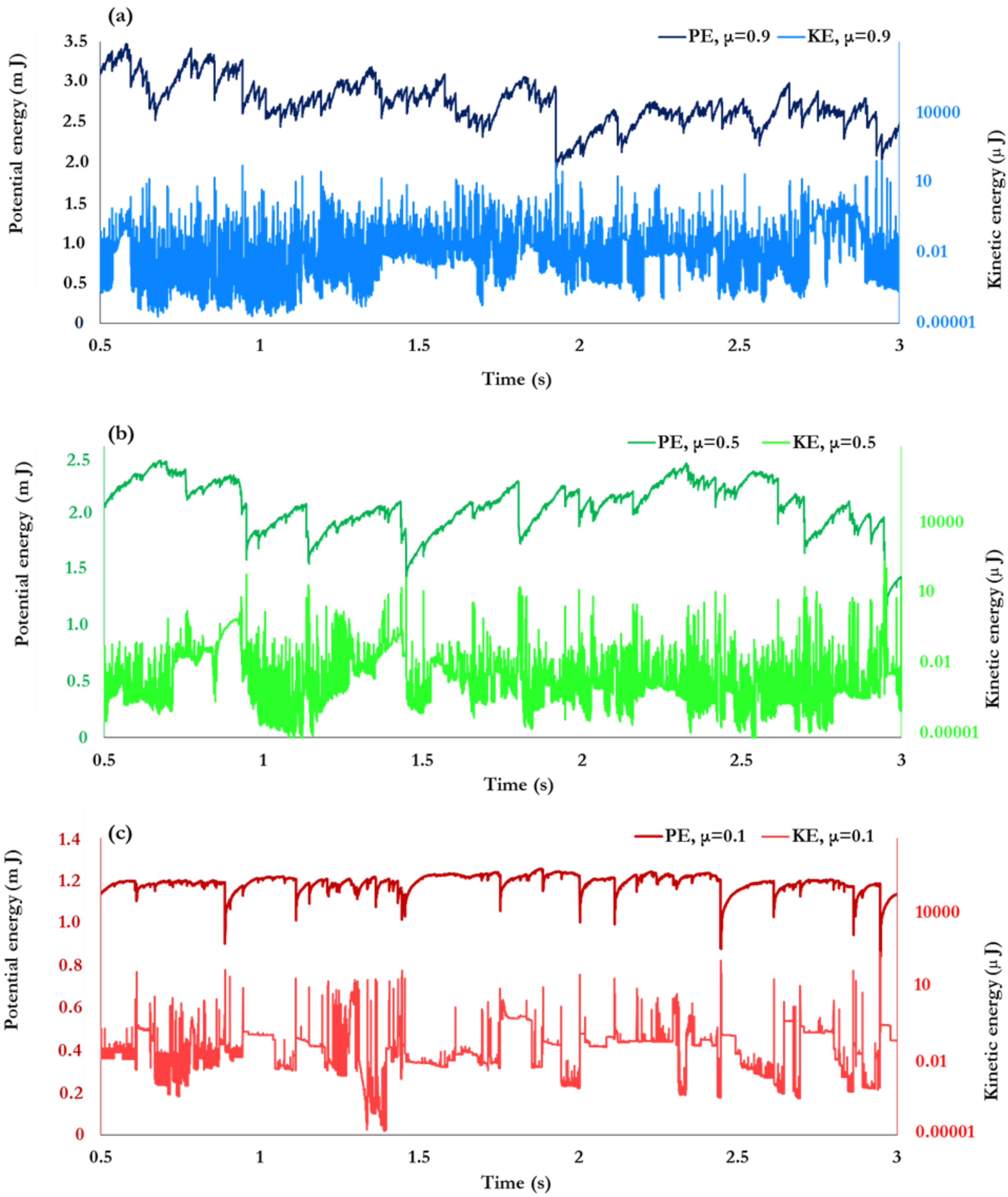

Fig. 8: (a-c) Evolution of potential energy (primary axis, left) and kinetic energy (secondary logarithmic axis, right) for particle friction values of 0.9, 0.5 and 0.1, respectively.

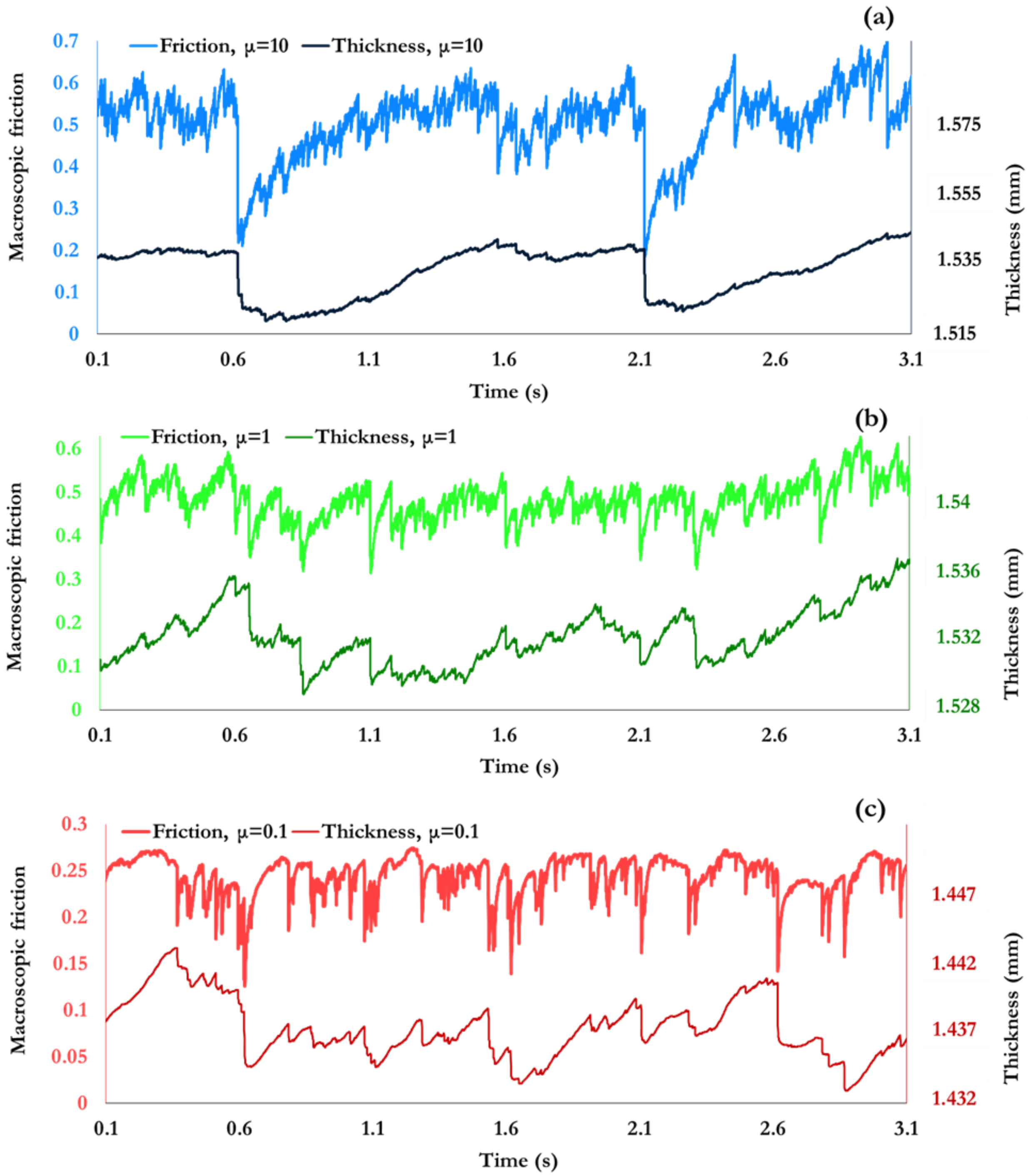

Fig. 9: (a-c) Time series of macroscopic friction (primary axis, left) and gouge thickness (secondary axis, right) for particle friction values of 10, 1, 0.1 respectively.

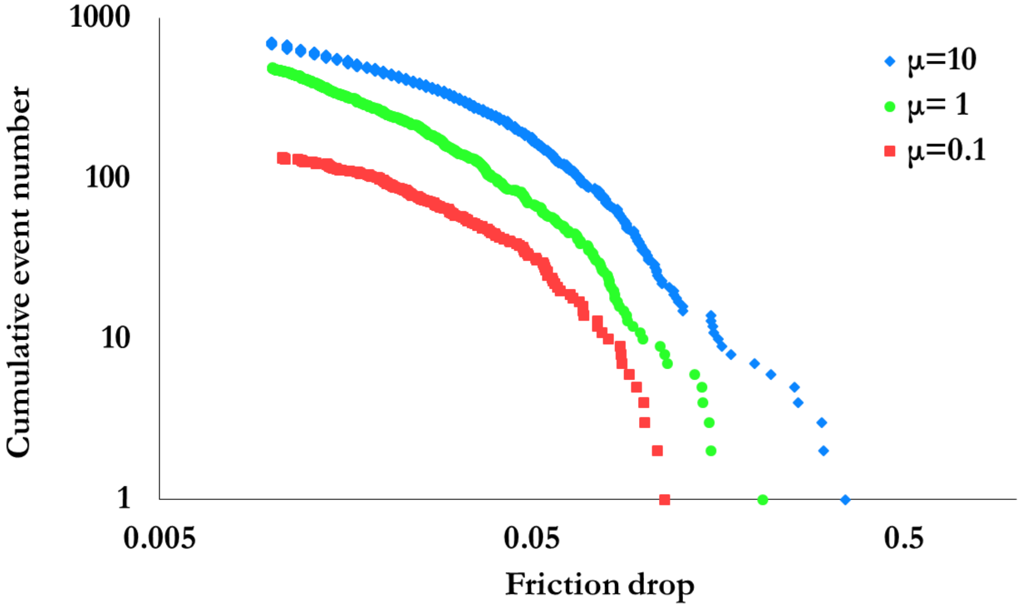

Fig. 10: Cumulative number of slip events versus macroscopic friction drop for different particle frictions of 10, 1 and 0.1.

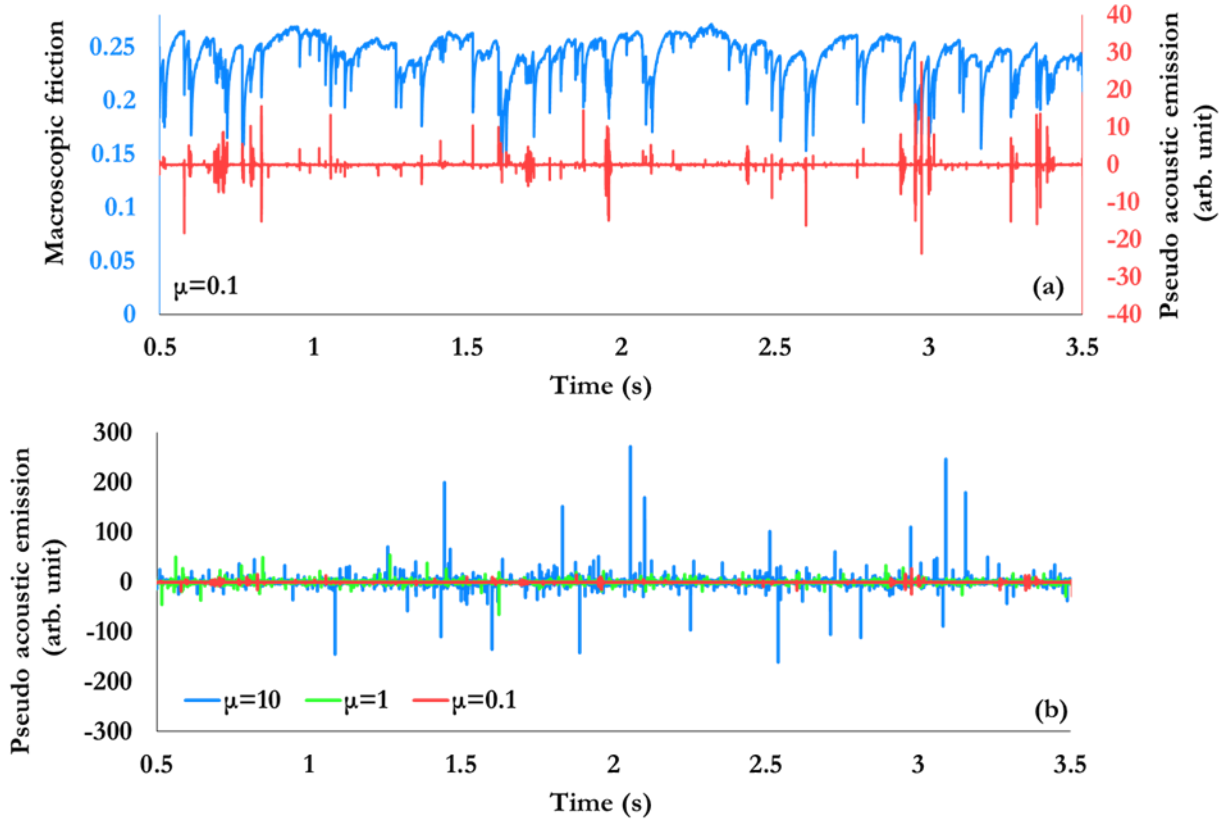

Fig. 11: (a) Macroscopic friction (primary axis, left) and pseudo acoustic emission (secondary axis, right) for particle friction values of 10, 1 and 0.1. (b) Time series of pseudo acoustic emission for particle friction values of 10, 1 and 0.1.

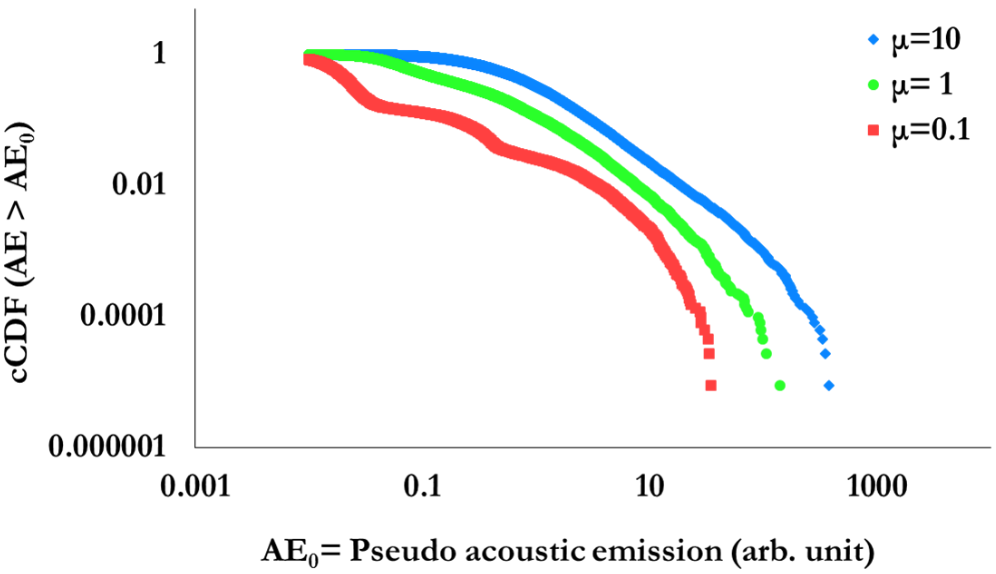

Fig. 12: Complementary Cumulative Distribution Function of pseudo acoustic emission for different particle friction values of 10, 1 and 0.1.

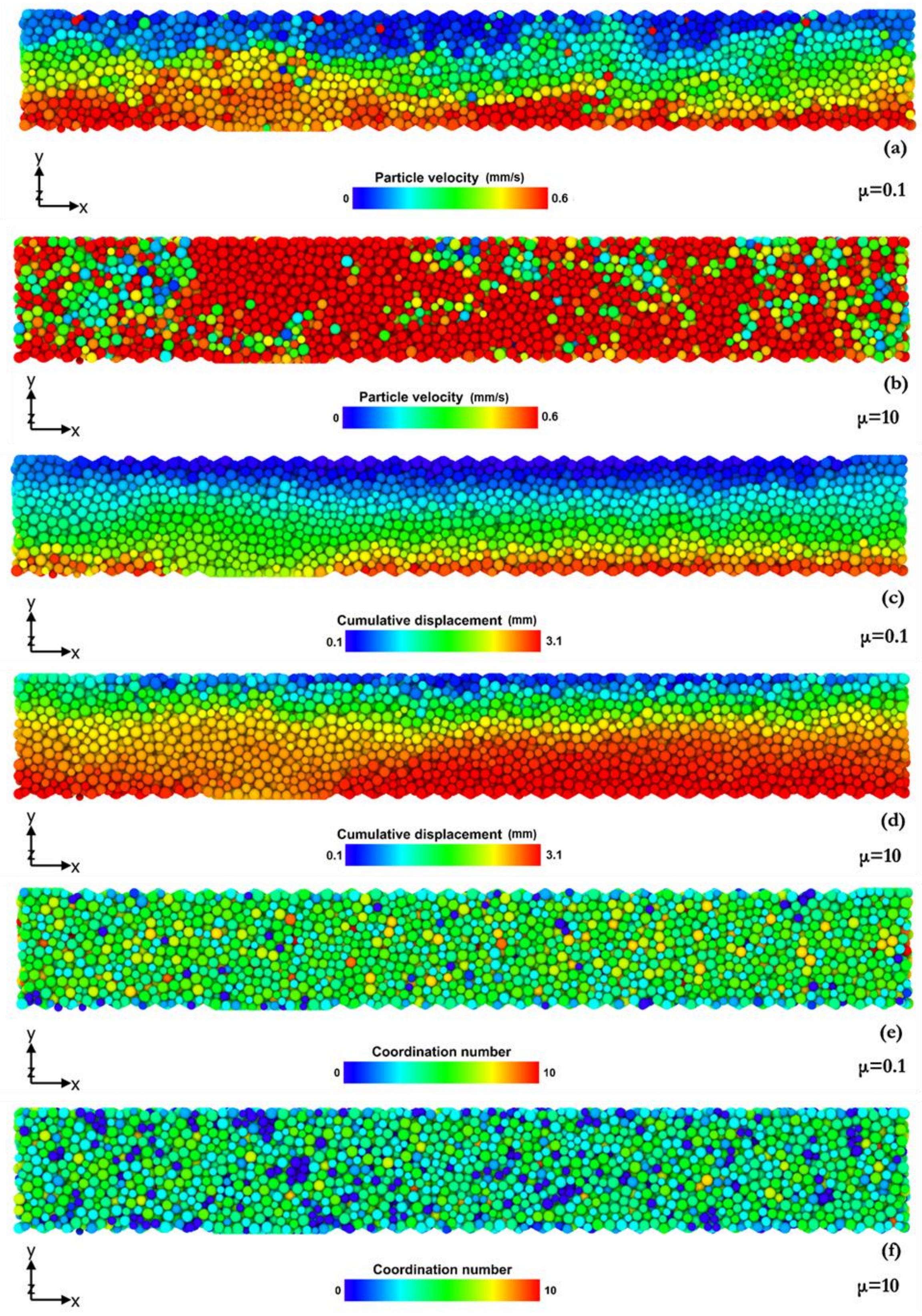

Fig. 13: (a, c, e) Spatial distribution of particle velocity, cumulative displacement and coordination number for particle friction values of 0.1 and (b, d, f) for particle friction of 10, respectively.

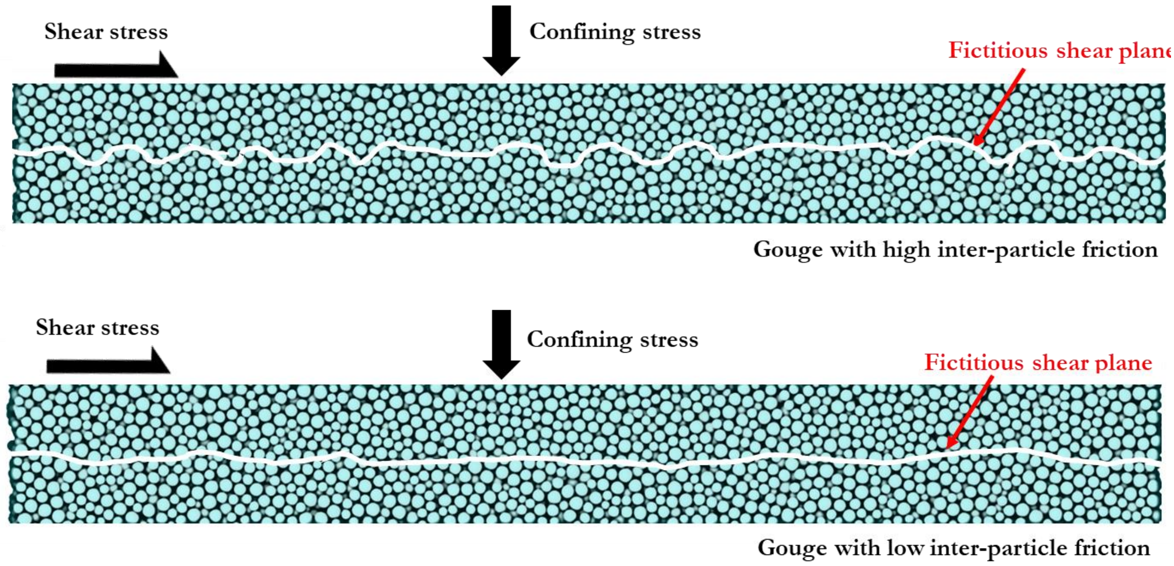

Fig. 14: Schematics of a fictitious shear plane at the core of fault gouge with low and high particle friction. The fictitious shear plane that is shown here with a curved line is a vast simplification of a complex 3D failure surface or an irregular failure pattern. The schematics delivers the hypothesis that high particle friction originates a more complex shear pattern that affects the mechanics of fault and characteristics of seismic cycles similar to the effect of fault surface roughness in absence of granular gouge.

8- References

Agnolin, I., & Roux, J. N. (2007). Internal states of model isotropic granular packings. I. Assembling process, geometry, and contact networks. *Physical Review E, 76*(6). doi:10.1103/PhysRevE.76.061302

Angheluta, L., Candela, T., Mathiesen, J., & Renard, F. (2011). Effect of Surface Morphology on the Dissipation During Shear and Slip Along a Rock–Rock Interface that Contains a Visco-elastic Core. *Pure and Applied Geophysics, 168*(12), 2335-2344. doi:10.1007/s00024-011-0272-8

Anthony, J. L., & Marone, C. (2005). Influence of particle characteristics on granular friction. *Journal of Geophysical Research-Solid Earth, 110*(B8). doi:10.1029/2004jb003399

Azéma, E., Estrada, N., Preechawuttipong, I., Delenne, J.-Y., & Radjai, F. (2017). Systematic description of the effect of particle shape on the strength properties of granular media. *EPJ Web Conf., 140*, 06026.

Azéma, E., Estrada, N., & Radjaï, F. (2012). Nonlinear effects of particle shape angularity in sheared granular media. *Physical Review E, 86*(4), 041301. doi:10.1103/PhysRevE.86.041301

Bistacchi, A., Griffith, W. A., Smith, S. A. F., Di Toro, G., Jones, R., & Nielsen, S. (2011). Fault Roughness at Seismogenic Depths from LIDAR and Photogrammetric Analysis. *Pure and Applied Geophysics, 168*(12), 2345-2363. doi:10.1007/s00024-011-0301-7

Bouchon, M., Karabulut, H., Bouin, M.-P., Schmittbuhl, J., Vallée, M., Archuleta, R., . . . Marsan, D. (2010). Faulting characteristics of supershear earthquakes. *Tectonophysics, 493*(3), 244-253. doi:https://doi.org/10.1016/j.tecto.2010.06.011

Brantut, N., Schubnel, A., Rouzaud, J. N., Brunet, F., & Shimamoto, T. (2008). High-velocity frictional properties of a clay-bearing fault gouge and implications for earthquake mechanics. *Journal of Geophysical Research: Solid Earth, 113*(B10). doi:10.1029/2007JB005551

Brodsky, E. E., Gilchrist, J. J., Sagy, A., & Collettini, C. (2011). Faults smooth gradually as a function of slip. *Earth and Planetary Science Letters, 302*(1), 185-193. doi:https://doi.org/10.1016/j.epsl.2010.12.010

Brodsky, E. E., Kirkpatrick, J. D., & Candela, T. (2016). Constraints from fault roughness on the scale-dependent strength of rocks. *Geology, 44*(1), 19-22.

Bruhat, L., Fang, Z., & Dunham, E. M. (2016). Rupture complexity and the supershear transition on rough faults. *Journal of Geophysical Research: Solid Earth, 121*(1), 210-224. doi:doi:10.1002/2015JB012512

Candela, T., Renard, F., Bouchon, M., Brouste, A., Marsan, D., Schmittbuhl, J., & Voisin, C. (2009). Characterization of Fault Roughness at Various Scales: Implications of Three-Dimensional High Resolution Topography Measurements. *Pure and Applied Geophysics, 166*(10), 1817-1851. doi:10.1007/s00024-009-0521-2

Candela, T., Renard, F., Bouchon, M., Schmittbuhl, J., & Brodsky, E. E. (2011). Stress drop during earthquakes: effect of fault roughness scaling. *Bulletin of the Seismological Society of America, 101*(5), 2369-2387.

Candela, T., Renard, F., Klinger, Y., Mair, K., Schmittbuhl, J., & Brodsky, E. E. (2012). Roughness of fault surfaces over nine decades of length scales. *Journal of Geophysical Research: Solid Earth, 117*(B8). doi:doi:10.1029/2011JB009041

Candela, T., Renard, F., Schmittbuhl, J., Bouchon, M., & Brodsky, E. E. (2011). Fault slip distribution and fault roughness. *Geophysical Journal International, 187*(2), 959-968. doi:10.1111/j.1365-246X.2011.05189.x

Cashman, S., & Cashman, K. (2000). Cataclasis and deformation-band formation in unconsolidated marine terrace sand, Humboldt County, California. *Geology, 28*(2), 111-114. doi:10.1130/0091-7613(2000)28<111:CADFIU>2.0.CO;2

Cashman, S. M., Baldwin, J. N., Cashman, K. V., Swanson, K., & Crawford, R. (2007). Microstructures developed by coseismic and aseismic faulting in near-surface sediments, San Andreas fault, California. *Geology, 35*(7), 611-614.

Chester, F. M., & Chester, J. S. (1998). Ultracataclasite structure and friction processes of the Punchbowl fault, San Andreas system, California. *Tectonophysics, 295*(1), 199-221. doi:https://doi.org/10.1016/S0040-1951(98)00121-8

Chester, F. M., & Chester, J. S. (2000). Stress and deformation along wavy frictional faults. *Journal of Geophysical Research: Solid Earth, 105*(B10), 23421-23430. doi:doi:10.1029/2000JB900241

Chester, F. M., Friedman, M., & Logan, J. M. (1985). Foliated cataclasites. *Tectonophysics, 111*(1), 139-146. doi:https://doi.org/10.1016/0040-1951(85)90071-X

Chester, F. M., & Logan, J. M. (1986). Implications for mechanical properties of brittle faults from observations of the Punchbowl fault zone, California. *pure and applied geophysics, 124*(1), 79-106. doi:10.1007/bf00875720

Di Renzo, A., & Di Maio, F. P. (2004). Comparison of contact-force models for the simulation of collisions in DEM-based granular flow codes. *Chemical Engineering Science, 59*(3), 525-541. doi:10.1016/j.ces.2003.09.037

Dieterich, J. H., & Kilgore, B. D. (1994). Direct observation of frictional contacts: New insights for state-dependent properties. *pure and applied geophysics, 143*(1), 283-302. doi:10.1007/bf00874332

Dieterich, J. H., & Smith, D. E. (2009). Nonplanar Faults: Mechanics of Slip and Off-fault Damage. *Pure and Applied Geophysics, 166*(10), 1799-1815. doi:10.1007/s00024-009-0517-y

Dorostkar, O. (2018). *Stick-slip dynamics in dry and fluid saturated granular fault gouge investigated by numerical simulations.* (PhD dissertaion), PhD dissertaion, ETH Zurich.,

Dorostkar, O., & Carmeliet, J. (2018). Potential Energy as Metric for Understanding Stick–Slip Dynamics in Sheared Granular Fault Gouge: A Coupled CFD–DEM Study. *Rock Mechanics and Rock Engineering*. doi:10.1007/s00603-018-1457-6

Dorostkar, O., Guyer, R. A., Johnson, P. A., Marone, C., & Carmeliet, J. (2017a). On the micromechanics of slip events in sheared, fluid saturated fault gouge. *Geophysical Research Letters*, 6101–6108. doi:10.1002/2017GL073768

Dorostkar, O., Guyer, R. A., Johnson, P. A., Marone, C., & Carmeliet, J. (2017b). On the role of fluids in stick-slip dynamics of saturated granular fault gouge using a coupled computational fluid dynamics-discrete element approach. *Journal of Geophysical Research: Solid Earth*. doi:10.1002/2017JB014099

Dorostkar, O., Guyer, R. A., Johnson, P. A., Marone, C., & Carmeliet, J. (2018). Cohesion-induced stabilization in stick-slip dynamics of weakly wet, sheared granular fault gouge. *Journal of Geophysical Research: Solid Earth*. doi:10.1002/2017JB015171

Dorostkar, O., Johnson, P., Guyer, R., Marone, C., & Carmeliet, J. (2017). Do Fluids Modify the Stick-Slip Behavior of Sheared Granular Media? *Poromechanics VI : Proceedings of the Sixth Biot Conference on Poromechanics, 2017.* , 158-163. doi:10.1061/9780784480779.019

Dunham, E. M., Belanger, D., Cong, L., & Kozdon, J. E. (2011). Earthquake ruptures with strongly rate-weakening friction and off-fault plasticity, Part 2: Nonplanar faults. *Bulletin of the Seismological Society of America, 101*(5), 2308-2322.

Engelder, J. T. (1974). Cataclasis and the Generation of Fault Gouge. *GSA Bulletin, 85*(10), 1515-1522. doi:10.1130/0016-7606(1974)85<1515:CATGOF>2.0.CO;2

Faulkner, D. R., Lewis, A. C., & Rutter, E. H. (2003). On the internal structure and mechanics of large strike-slip fault zones: field observations of the Carboneras fault in southeastern Spain. *Tectonophysics, 367*(3), 235-251. doi:https://doi.org/10.1016/S0040-1951(03)00134-3

Fournier, T., & Morgan, J. (2012). Insights to slip behavior on rough faults using discrete element modeling. *Geophysical Research Letters, 39*(12). doi:doi:10.1029/2012GL051899

Frye, K. M., & Marone, C. (2002). Effect of humidity on granular friction at room temperature. *Journal of Geophysical Research-Solid Earth, 107*(B11). doi:10.1029/2001jb000654

Goebel, T. H. W., Becker, T. W., Sammis, C. G., Dresen, G., & Schorlemmer, D. (2014). Off-fault damage and acoustic emission distributions during the evolution of structurally complex faults over series of stick-slip events. *Geophysical Journal International, 197*(3), 1705-1718. doi:10.1093/gji/ggu074

Goebel, T. H. W., Becker, T. W., Schorlemmer, D., Stanchits, S., Sammis, C., Rybacki, E., & Dresen, G. (2012). Identifying fault heterogeneity through mapping spatial anomalies in acoustic emission statistics. *Journal of Geophysical Research: Solid Earth, 117*(B3). doi:doi:10.1029/2011JB008763

Goebel, T. H. W., Candela, T., Sammis, C. G., Becker, T. W., Dresen, G., & Schorlemmer, D. (2014). Seismic event distributions and off-fault damage during frictional sliding of saw-cut surfaces with pre-defined roughness. *Geophysical Journal International, 196*(1), 612-625. doi:10.1093/gji/ggt401

Goebel, T. H. W., Kwiatek, G., Becker, T. W., Brodsky, E. E., & Dresen, G. (2017). What allows seismic events to grow big?: Insights from b-value and fault roughness analysis in laboratory stick-slip experiments. *Geology, 45*(9), 815-818. doi:10.1130/G39147.1

Göncü, F., & Luding, S. (2013). Effect of particle friction and polydispersity on the macroscopic stress–strain relations of granular materials. *Acta Geotechnica, 8*(6), 629-643. doi:10.1007/s11440-013-0258-z

Goniva, C., Kloss, C., Deen, N. G., Kuipers, J. A. M., & Pirker, S. (2012). Influence of rolling friction on single spout fluidized bed simulation. *Particuology, 10*(5), 582-591. doi:10.1016/j.partic.2012.05.002

Haines, S., Marone, C., & Saffer, D. (2014). Frictional properties of low-angle normal fault gouges and implications for low-angle normal fault slip. *Earth and Planetary Science Letters, 408*, 57-65. doi:10.1016/j.epsl.2014.09.034

Heermance, R., Shipton, Z. K., & Evans, J. P. (2003). Fault Structure Control on Fault Slip and Ground Motion during the 1999 Rupture of the Chelungpu

Fault, Taiwan. *Bulletin of the Seismological Society of America, 93*(3), 1034-1050. doi:10.1785/0120010230

Hertz, H. (1882). Ueber die Berührung fester elastischer Körper. *Journal für die reine und angewandte Mathematik, 92*, 156-171.

J. Latham, S., Abe, S., & R. Mora, P. (2005). *Macroscopic Friction Response of Rotational and Non-Rotational Lattice Solid Gouge Models in 2D and 3D.* Paper presented at the Powders and Grains 2005, Stuttgart, Germany.

Karner, S. L., & Marone, C. (2000). Effects of Loading Rate and Normal Stress on Stress Drop and Stick-Slip Recurrence Interval. *GeoComplexity and the Physics of Earthquakes*, 187-198.

Kloss, C., Goniva, C., Hager, A., Amberger, S., & Pirker, S. (2012). Models, algorithms and validation for opensource DEM and CFD-DEM. *Progress in Computational Fluid Dynamics, 12*(2-3), 140-152.

Knuth, M., & Marone, C. (2007). Friction of sheared granular layers: Role of particle dimensionality, surface roughness, and material properties. *Geochemistry, Geophysics, Geosystems, 8*(3). doi:doi:10.1029/2006GC001327

Kozłowska, M., Brudzinski, M. R., Friberg, P., Skoumal, R. J., Baxter, N. D., & Currie, B. S. (2018). Maturity of nearby faults influences seismic hazard from hydraulic fracturing. *Proceedings of the National Academy of Sciences, 115*(8), E1720-E1729. doi:10.1073/pnas.1715284115

Kwiatek, G., Goebel, T. H. W., & Dresen, G. (2014). Seismic moment tensor and b value variations over successive seismic cycles in laboratory stick-slip experiments. *Geophysical Research Letters, 41*(16), 5838-5846. doi:doi:10.1002/2014GL060159

Mair, K., Frye, K. M., & Marone, C. (2002). Influence of grain characteristics on the friction of granular shear zones. *Journal of Geophysical Research-Solid Earth, 107*(B10). doi:10.1029/2001jb000516

Makedonska, N., Sparks, D. W., Aharonov, E., & Goren, L. (2011). Friction versus dilation revisited: Insights from theoretical and numerical models. *Journal of Geophysical Research, 116*(B9). doi:10.1029/2010jb008139

Marone, C. (1998). The effect of loading rate on static friction and the rate of fault healing during the earthquake cycle. *Nature, 391*(6662), 69-72.

Marone, C. (1998). Laboratory-derived friction laws and their application to seismic faulting. *Annual Review of Earth and Planetary Sciences, 26*, 643-696. doi:10.1146/annurev.earth.26.1.643

Marone, C., Raleigh, C. B., & Scholz, C. H. (1990). Frictional behavior and constitutive modeling of simulated fault gouge. *Journal of Geophysical Research-Solid Earth and Planets, 95*(B5), 7007-7025. doi:10.1029/JB095iB05p07007

McLaskey, G. C., & Glaser, S. D. (2011). Micromechanics of asperity rupture during laboratory stick slip experiments. *Geophysical Research Letters, 38*(12). doi:doi:10.1029/2011GL047507

Mead, W. J. (1925). The geologic role of dilatancy. *The Journal of Geology, 33*(7), 685-698.

MiDi, G. D. R. (2004). On dense granular flows. *European Physical Journal E, 14*(4), 341-365. doi:10.1140/epje/i2003-10153-0

Ohnaka, M. (2003). A constitutive scaling law and a unified comprehension for frictional slip failure, shear fracture of intact rock, and earthquake rupture. *Journal of Geophysical Research: Solid Earth, 108*(B2). doi:doi:10.1029/2000JB000123

Ohnaka, M., & Shen, L.-f. (1999). Scaling of the shear rupture process from nucleation to dynamic propagation: Implications of geometric irregularity of the rupturing surfaces. *Journal of Geophysical Research: Solid Earth, 104*(B1), 817-844. doi:doi:10.1029/1998JB900007

Rathbun, A. P., & Marone, C. (2010). Effect of strain localization on frictional behavior of sheared granular materials. *Journal of Geophysical Research, 115*(B1). doi:10.1029/2009jb006466

Rathbun, A. P., Renard, F., & Abe, S. (2013). Numerical investigation of the interplay between wall geometry and friction in granular fault gouge. *Journal of Geophysical Research: Solid Earth, 118*(3), 878-896. doi:doi:10.1002/jgrb.50106

Renard, F., Voisin, C., Marsan, D., & Schmittbuhl, J. (2006). High resolution 3D laser scanner measurements of a strike-slip fault quantify its morphological anisotropy at all scales. *Geophysical Research Letters, 33*(4). doi:doi:10.1029/2005GL025038

Rijsingen, E., Lallemand, S., Peyret, M., Arcay, D., Heuret, A., Funiciello, F., & Corbi, F. (2018). How subduction interface roughness influences the occurrence of large interplate earthquakes. *Geochemistry, Geophysics, Geosystems*. doi:doi:10.1029/2018GC007618

Rivière, J., Lv, Z., Johnson, P. A., & Marone, C. (2018). Evolution of b-value during the seismic cycle: Insights from laboratory experiments on simulated faults. *Earth and Planetary Science Letters, 482*, 407-413. doi:https://doi.org/10.1016/j.epsl.2017.11.036

Rosenau, M., Corbi, F., & Dominguez, S. (2017). Analogue earthquakes and seismic cycles: experimental modelling across timescales. *Solid Earth, 8*(3), 597-635. doi:10.5194/se-8-597-2017

Rouet-Leduc, B., Hulbert, C., Lubbers, N., Barros, K., Humphreys, C. J., & Johnson, P. A. (2017). Machine Learning Predicts Laboratory Earthquakes. *Geophysical Research Letters, 44*(18), 9276-9282. doi:10.1002/2017GL074677

Sagy, A., Brodsky, E. E., & Axen, G. J. (2007). Evolution of fault-surface roughness with slip. *Geology, 35*(3), 283-286. doi:10.1130/G23235A.1

Sheng, Y., Lawrence, C. J., Briscoe, B. J., & Thornton, C. (2004). Numerical studies of uniaxial powder compaction process by 3D DEM. *Engineering Computations, 21*(2-4), 304-317. doi:10.1108/02644400410519802

Shimamoto, T. (1979). *Experimental studies of simulated gouge and their application to studies of natural fault zones*. Paper presented at the Conference VIII: Analysis of Actual Fault Zones in Bedrock, Natl. Earthquake Hazards Reduct. Program, Menlo Park, Calif.

Shojaaee, Z., Brendel, L., Török, J., & Wolf, D. E. (2012). Shear flow of dense granular materials near smooth walls. II. Block formation and suppression of slip by rolling friction. *Physical Review E, 86*(1), 011302. doi:10.1103/PhysRevE.86.011302

Tal, Y., & Hager, B. H. (2018). The Slip Behavior and Source Parameters for Spontaneous Slip Events on Rough Faults Subjected to Slow Tectonic Loading. *Journal of Geophysical Research: Solid Earth, 123*(2), 1810-1823. doi:doi:10.1002/2017JB014737

Tal, Y., Hager, B. H., & Ampuero, J. P. (2018). The Effects of Fault Roughness on the Earthquake Nucleation Process. *Journal of Geophysical Research: Solid Earth, 123*(1), 437-456. doi:doi:10.1002/2017JB014746

Wang, K., & Bilek, S. L. (2014). Invited review paper: Fault creep caused by subduction of rough seafloor relief. *Tectonophysics, 610*, 1-24. doi:https://doi.org/10.1016/j.tecto.2013.11.024

Zielke, O., Galis, M., & Mai, P. M. (2017). Fault roughness and strength heterogeneity control earthquake size and stress drop. *Geophysical Research Letters, 44*(2), 777-783. doi:doi:10.1002/2016GL071700

Zoback, M., Hickman, S., & Ellsworth, W. (2010). Scientific drilling into the San Andreas fault zone. *Eos, Transactions American Geophysical Union, 91*(22), 197-199.